

https://dspace.org/

Biomass valorisation of marula nutshell waste into nitrogen-doped activated carbon for use in high performance supercapacitors

Shaku, B.; Mofokeng, T.P.; Coville, N.J.; Ozoemena, K.I.; Maubane-Nkadimeng, M.S.

2023-01
Elsevier
https://hdl.handle.net/10539/49849
B. Shaku, T.P. Mofokeng, N.J. Coville, K.I. Ozoemena, M.S. Maubane-Nkadimeng, Biomass valorisation of marula nutshell waste into nitrogen-doped activated carbon for use in high performance supercapacitors, Electrochimica Acta, Volume 442, 2023, 141828, ISSN 0013-4686, https://doi.org/10.1016/j.electacta.2023.141828.

Downloaded from a DSpace repository. https://dspace.org/

Electrochimica Acta 442 (2023) 141828



Contents lists available at ScienceDirect

Electrochimica Acta

journal homepage: www.journals.elsevier.com/electrochimica-acta





Biomass valorisation of marula nutshell waste into nitrogen-doped activated carbon for use in high performance supercapacitors

B. Shaku [a,b], T.P. Mofokeng [a,b], N.J. Coville [a,b], K.I. Ozoemena [a,b,*], M.S. Maubane-Nkadimeng [a,b,c,*]

[a] DSI-NRF Centre of Excellence in Strong Materials, University of the Witwatersrand, Private Bag 3, Johannesburg 2050, South Africa
[b] Molecular Sciences Institute, School of Chemistry, University of the Witwatersrand, Private Bag 3, Johannesburg 2050, South Africa
[c] Microscopy and Microanalysis Unit, University of the Witwatersrand, private Bag 3, Johannesburg, South Africa

ARTICLE INFO

Keywords:
Marula nutshells
KOH activation
Nitrogen doping
Supercapacitors

ABSTRACT

This study reports on the valorisation of marula nutshell waste into a valuable electrode material for supercapacitors. Marula nutshell waste, a brown hard residue from marula fruits was valorised into a nitrogen-doped activated carbon (N-ACs) by KOH treatment and using melamine as a nitrogen source. The microporous and mesoporous nature of N-ACs exhibited a high surface area of 1427 m^2 g^{-1} and pore volume of 0.31 cm^3 g^{-1}. Three electrode measurements were done in 6 M KOH and 2.5 M KNO_3 aqueous electrolytes, to examine the materials in alkaline and neutral medium. The N-ACs exhibited a capacitance of 350 F g^{-1} in 6 M KOH and 248 F g^{-1} in 2.5 M KNO_3 electrolyte. Due to low toxicity and wider operating voltage (~1.8 V) of 2.5 KNO_3, the material was further analysed in a symmetric device. The high surface area, the defects, and the high content of nitrogen (5.1%) revealed that the material produced an outstanding energy density of 17.2 Wh kg^{-1} and a power density of 448.7 W kg^{-1} in 2.5 M KNO_3 electrolyte. The conversion of marula nuts waste into N-ACs thus provide a means of converting biomass waste into a useful energy storage material for supercapacitors.

1. Introduction

The sustainability of human development through the generation of energy by 'green' methodologies is a tremendous challenge and requires the development of efficient, safe, and high-performance energy storage devices [1–3]. Hence, much research has been undertaken to develop supercapacitors (SCs) for high powered energy storage as one solution to solve this problem [4,5]. Electric double layer capacitors (EDLCs) store charge by a simple ion-adsorption process (non-faradic) at an electrode/electrolyte interface [6,7]. EDLCs have been shown to have fast charging-discharging rates and a long life cycle which makes them useful as high powered devices [8,9]. The efficiency of SCs as electrochemical cells depend on the type of electrode material used. One material that has been extensively studied as an electrode material in SCs is activated carbons (ACs) because of its low cost, high specific surface area (SSA) and high thermal stability [10,11]. Precursors for making ACs and their optimum synthesis conditions require careful selection in order to achieve desirable properties. Precursors for making ACs commercially are derived from fossil fuels such as coal, polymers, and pitch which can be expensive and/or ecologically unfriendly. Therefore, there is a need to determine whether the synthesis of ACs from renewable waste carbon containing sources that are cheap is possible. The ACs produced will need to compete with ACs produced from waste (i.e. pomelo peel [12], hazel nutshell [13] etc.) in terms of physical properties, reproducibility and cost. Here we report on the use of a local waste, marula nutshells which is found in abundance in South Africa for use as an electrode material making nitrogen doped activated carbons by KOH and melamine (for the first time) in SCs.

South Africa is one of the largest producers of marula fruits, and these fruits are used for producing the international branded Amarula liquour (Distell production, South Africa) [14]. Sclerocarya birrea (marula) produces the fruits in warm frost-free climates, as found in the Northern parts of South Africa. The tree can produce 500 kg of ripe fruits per year with a delightfully juicy acid taste. The fruit contains nut that is removed from the fruit and this marula nutshell generates a waste that is pale brown in colour and has an oval shape [15]. Marula nutshell has been reported to have a carbon content of ~38.2%, a moisture content of ~5.5% and an ash content of ~8.4% [16]. The low ash content

* Corresponding authors.
E-mail addresses: kenneth.ozoemena@wits.ac.za (K.I. Ozoemena), manoko.maubane@wits.ac.za (M.S. Maubane-Nkadimeng).

https://doi.org/10.1016/j.electacta.2023.141828
Received 6 September 2022; Received in revised form 23 December 2022; Accepted 1 January 2023
Available online 2 January 2023
0013-4686/© 2023 The Authors. Published by Elsevier Ltd. This is an open access article under the CC BY-NC-ND license (http://creativecommons.org/licenses/by-nc-nd/4.0/).

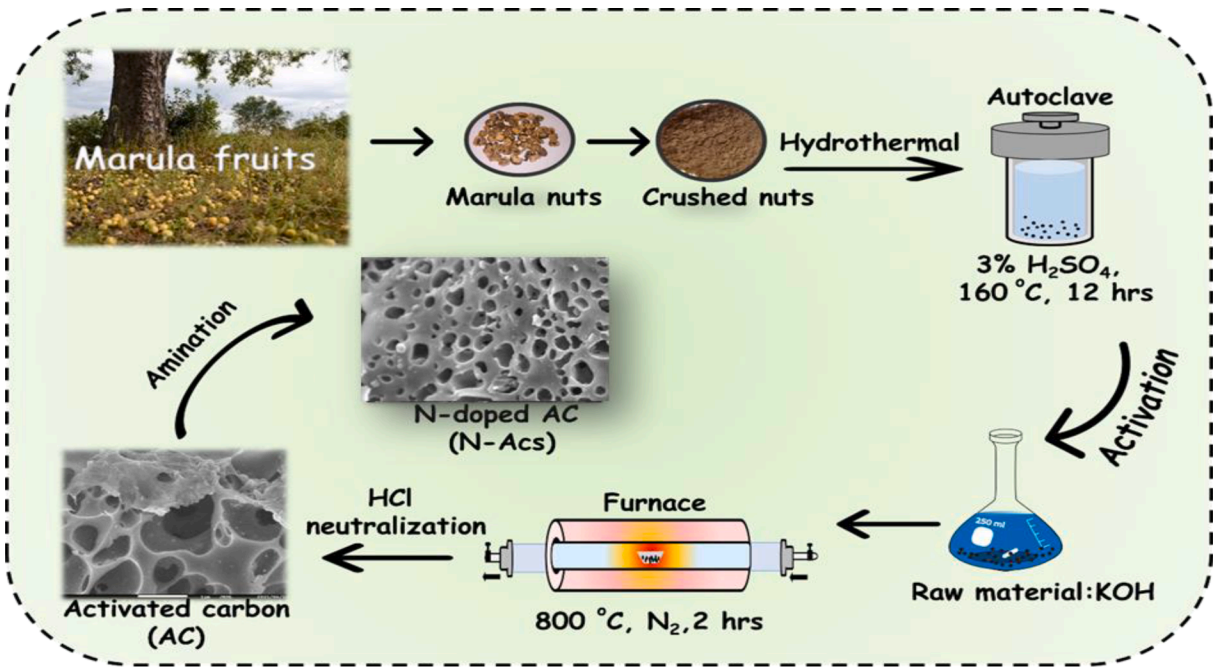


Fig. 1. A schematic depicting the synthetic route to make the activated carbons and nitrogen doped activated carbons.

present in the biomass has been reported to have good properties for making good adsorbent ACs with good mechanical strength [16].

Studies of ACs as electrode materials for SCs have shown some limitations. For example, the type of biomass and different precursors used during synthesis can impact on its properties [17]. ACs can be synthesized from different methods such as physical/chemical activation and microwave irradiation [18,19]. Microwave irradiations are used to heat dielectric materials [20]. Physical activation normally involves pyrolysis at higher temperature (> 500 °C) followed by activation at higher temperatures (700–1000 °C) using activating agents such as air, CO_2 and steam [21]. Chemical activation involves treatment of the biomass with an activating agent followed by pyrolysis leading to efficient porosity of the material [22,23].

Regardless of the method, the improvement of the energy efficiency of the ACs is very important due to the low conductivity of the carbon materials resulting from degree of carbon graphitization. This low conductivity produces a limited amount of energy storage due to the restriction of fast charging-discharging rates [24]. Heteroatom species such as nitrogen, boron, sulphur etc. can be introduced into the carbon matrix to overcome the low conductivity associated with the ACs [25,26]. In particular, the introduction of nitrogen on, or into, the carbon matrix improves the capacitance due to the enhanced wettability of the material, thus improving the electric contact between the electrode and electrolyte [27,28]. Nitrogen-doped carbons can be synthesized by in-situ or ex-situ thermal processes using nitrogen containing species such as ammonia gas (NH_3), melamine, urea, acetonitrile etc. [29,30]. In-situ nitrogen doping involves a one or two pot synthesis. In the one pot synthesis of the biomass, an activating agent and a nitrogen source are mixed together and then carbonized. In the two pot synthesis direct pyrolysis of the material in the presence of a nitrogen containing species followed by activation at high temperatures is used [31,32].

For example, Ahmed et al. [31] reported on the in-situ nitrogen doping of orange peel as a biomass at 700 °C, using melamine as a nitrogen source and KOH as an activating agent. The nitrogen content decreased as the KOH concentration increased with a highest capacitance of 168 F/g exhibited at 10 mV s^{-1} with an energy density of 5.79 Wh kg^{-1} in 6 M KOH electrolyte. Zhou et al. [33] reported on the formation of nitrogen doped porous carbons using ethylenediamine as a nitrogen source and carbon tetrachloride as a carbon source by KOH activation. The nitrogen doped porous carbon showed a decrease of the nitrogen content from 10.8% to 1.1% as the KOH concentration increased. In another study by Mo et al. [34], watermelon rind that contained nitrogen (~2.8%) was used to make ACs. After KOH impregnation, the surface area increased to 2277 m^2 g^{-1} but the nitrogen content decreased to 1.51% and the carbon electrode had a capacitance of 270 F g^{-1} in 6 M KOH electrolyte. The above studies revealed that the surface area and the nitrogen content are two complementary features that influence the SCs properties and that the use of elevated temperatures and increased KOH concentrations decrease the nitrogen content. An alternative method to produce ACs with a high surface area, and with moderate to high nitrogen-content, is by using ex-situ nitrogen doping i.e. the two-pot synthesis approach. Thus, in this study we have made nitrogen-doped ACs from the carbons produced from the marula nutshells that have a moderate nitrogen content and high surface area via the ex-situ two pot doping method.

Energy storage in SCs is not only dependent on active surface area and conductivity, but also the properties of the electrolyte [35]. Another way of increasing the energy density of a SC is by using organic or ionic electrolytes that operate over a wide voltage range [36,37]. However, it must be kept in mind that organic or ionic liquids suffer from poor conductivity compared to aqueous electrolytes although they have wide operating voltage and high viscosity creating hindrance charge accumulation of electrolyte ions [37]. Hence, aqueous electrolytes can be used because of the high conductivity.

Within this context, the objective of the study is to evaluate marula nutshell as a precursor electrode material for producing ACs under different impregnation ratios of the biomass and KOH. Marula fruits, besides being the main products for producing Amarula liqueur, the material produces marula nutshell which possess adequate characteristics for the production of activated carbon. In the literature, there are no published studies on obtaining nitrogen doped ACs from marula nutshell by KOH activation and melamine as a nitrogen precursor. To this purpose, using KOH as an activating agent and the effect of nitrogen has been investigated. Samples of the activated and nitrogen doped were subjected to electrochemical examination using a three-electrode system in 6 M KOH and 2.5 KNO_3 electrolyte. Due to the wider potential window of KNO_3 [38], the materials were further evaluated in a two electrode system. Neutral electrolytes are used because of their cost

Table 1
Abbreviations and compositions of activated carbons produced from marula nuts waste.

Abbreviation	PMNW:KOH (wt %)
AMNW-0.5	1:0.5
AMNW-1	1:1
AMNW-2	1:2
AMNW-3	1:3
PMNW	Hydrothermal treatment, no activation
MNW	No hydrothermal treatment, no activation
N-ACs	AMNW-2:melamine (1:3)

effectiveness, corrosion resistance, and electrochemical stability. They also make the EDLCs assembly a simple process [39]. Also, 2.5 M KNO_3 affirmed the possibility of expanding the potential range of the electrolyte to a wide range leading to an efficient capacitor.

2. Experimental section

2.1. Materials

Marula nut waste used in the experiment were collected from nuts found in the Limpopo province, Modimolle (South Africa). The N-ACs were synthesized using nitrogen (N_2; 99.9% Afrox), potassium hydroxide (KOH; Sigma Aldrich) and melamine (Sigma Aldrich). Microfiber filter paper (ACE chemicals) were used as an electrode separator with 0.18 mm thickness. All other reagents were used without further purification.

2.2. Synthesis of activated carbon

Fig. 1 shows a schematic representation of the synthesis of the ACs. Marula nuts waste (MNW) was washed with acetone and water to remove dirt and then pulverized into powder. The powdered material was sieved to have a size < 150 μm. About 10.0 g of the sieved material was treated hydrothermally in air in 3% H_2SO_4 using a heating rate of 5 °C min^{-1} to achieve the required temperature (160 °C, 12 h). This pre-treated material was then washed with distilled water until a neutral pH was achieved. The material was labelled pre-treated marula nuts waste (PMNW) [40]. About 4.0 g of the PMNW was added to KOH using different mass ratios (PMNW:KOH =1:0.5, 1:1, 1:2, 1:3) in 50 mL distilled water. The mixtures were stirred for 24 h at room temperature and oven dried overnight at 80 °C. About 3.0 g of the dried mixture was placed in a quartz boat in a furnace for 2 h at 800 °C (heating rate used: 5 °C min^{-1}) under a flow of nitrogen (250 ml min^{-1}). The resulting material was washed with 1.0 M HCl, followed by distilled water until neutral pH [41] (see Fig. 1). The PMNW samples were labelled activated marula nuts waste (AMNW-0.5, AMNW-1, AMNW-2, AMNW-3) respectively for the samples made using the different KOH mass ratios (PMNW:KOH =1:0.5, 1:1, 1:2, 1:3) (Table 1).

The final weight percentage of the activated materials was calculated using Eq. (1).

$$\%\text{yield} = \frac{m_f}{m_i} \times 100\% \quad (1)$$

where m_i is the initial mass before carbonization and activation, m_f is the final mass after the KOH synthesis step (Table S1).

2.3. Ex-situ nitrogen doping

Ex-situ nitrogen doping was achieved by mixing AMNW-2 with melamine (1 (AMNW-2):3 (melamine) in 20 mL distilled water (Fig. 1). The mixture was stirred for 2 h at room temperature and dried in an oven at 80 °C overight. The dried mixture was placed in a quartz boat in a furnace for 2 h at 800 °C (heating rate: 5 °C min^{-1}) under a flow of nitrogen (250 ml min^{-1}). The material was washed with distilled water. The resulting materials was labelled ex-situ nitrogen doped activated carbons (N-ACs) [42].

2.5. Electrochemical characterization

The working electrode was fabricated by mixing the activated materials (80%) with carbon black (CB, 10%) and polyvinylidene (PVDF, 10%) in a few drops of methylpyrrolidone (NMP) [43]. The slurry was sonicated for 30 min, pasted on carbon paper and dried in a vacuum oven at 60 °C for 12 h The coated carbon papers were used as working electrodes in the two- and three-electrode systems. The three-electrode system (half-cell) in 6 M KOH and 2.5 M KNO_3 was constructed using nickel foam as a counter electrode and saturated calomel electrode as a reference electrode in a T-type Swagelok cell. The two-electrode (full--cell) system was assembled using a T-type Swagelok cell with a microfiber filter paper between the electrodes that was soaked in a 2.5 M KNO_3 electrolyte. The total mass per unit area of active material was around ~1.1 cm^2 mg^{-1}. All the electrochemical analyses were tested by using cyclic voltammetry (CV), galvanostatic charge-discharge (GCD), and impedance spectroscopy (EIS) procedures using a SP300 potentiostat.

The specific capacitance (C_{sp}), energy density (E_s), power density (P_s) were calculated from the discharge time obtained from GCD curves using Eqs. (2)-(6) [44–48].

Eq. (2) was used to calculate capacitance (F):

$$C = \frac{I \times \Delta t}{\Delta V} \quad (2)$$

Where the discharge current is given by I/A, $\Delta t/s$ is the discharge time, $\Delta v/V$ is the potential difference.

Eq. (3) was used to calculate the specific capacitance, C_s/F g^{-1} of the three electrode/half-cell:

$$Csp = \frac{C}{m} \quad (3)$$

Where m(g) is the mass of the active electrode material.

The C_s/F g^{-1} for a full-cell/symmetric two electrode system, where the counter and working electrode are the same active material has been calculated using Eq. (4):

$$Csp = 4\,\frac{C}{m} \quad (4)$$

Where m/g is the total active electrode mass.

Energy density (E_s) 's basic expression in Eq. (5) is in the unit J g^{-1}.

$$Es = \frac{1}{2} \times C_{sp}(\Delta V)^2 \quad (5)$$

Where C_{sp}/ F g^{-1} is the specific capacitance and ΔV/V is the potential window. To convert J g^{-1} to unit Wh g^{-1}, Eq. (5) is divided by a factor of 3600. To convert to Wh kg^{-1}, the units are multiplied by a 1000 to give Eq. (6). Hence, Es/Wh kg^{-1} is given by Eq. (6) and P_s/W kg^{-1} is calculated from Eq. (7).

$$Es = \frac{1}{2} \times C_{sp}(\Delta V)^2 = \frac{C \times (\Delta V)^2}{2m} \times \frac{1000}{3600} \quad (6)$$

Where C is capacitance, ΔV/V is the cell potential and m/kg is the mass of both active electrodes.

Power density (P_s) was calculated from Eq. (7):

$$Ps = 3600\frac{E_s}{\Delta t} \quad (7)$$

3. Characterization techniques

The morphology of the synthesized materials were characterized by using scanning electron microscopy (SEM) measurements (LEO, Zeiss SEM). The defects present in the material were established by Raman

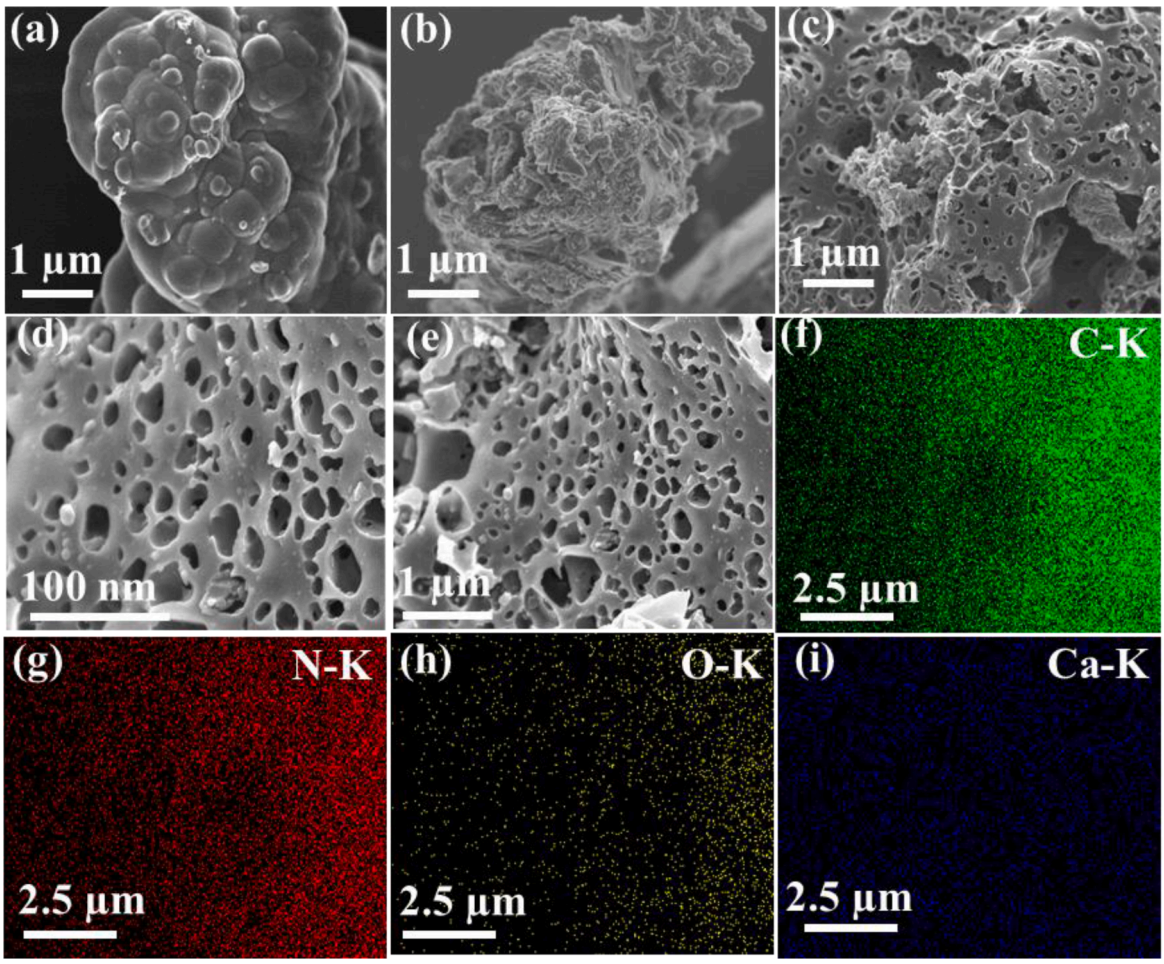


Fig. 2. SEM images of (a) MNW, (b) PMNW, (c) AMNW-2, (d) high, (e) low magnification of N-ACs and the corresponding EDS mapping of for the different elements: (f) C-K, (g) N-K, (h) O-K and (i) Ca-K.

spectroscopy (micro-Raman mode; Jobin-Yvon T64000, $\lambda = 532$ nm) at a focal plane of 1.5 µm. The surface area of the materials were determined using the Brunauer-Emmett-Teller (BET) procedure (Micrometrics Tristar 300 analyser). Thermal gravimetric analysis (TGA, Perkin Elmer 6000) was used to measure the stability of the materials. X-ray photoelectron spectroscopy (XPS) data was collected using a Physical Electronics Quantum 2000 instrument at 1486.7 eV using monochromatic a Al Kα source.

4. Results and discussion

4.1. Influence of PMNW:KOH ratio

The nut waste after acid treatment was treated with KOH. Different PMNW:KOH ratios were used (1:0.5, 1:1, 1:2, 1:3) based on earlier studies on similar carbons [49]. After the impregnation studies with KOH, the samples were heated at 800 °C for 2 h to obtain the desired material. As expected, carbon was lost under these conditions (Fig. S1).

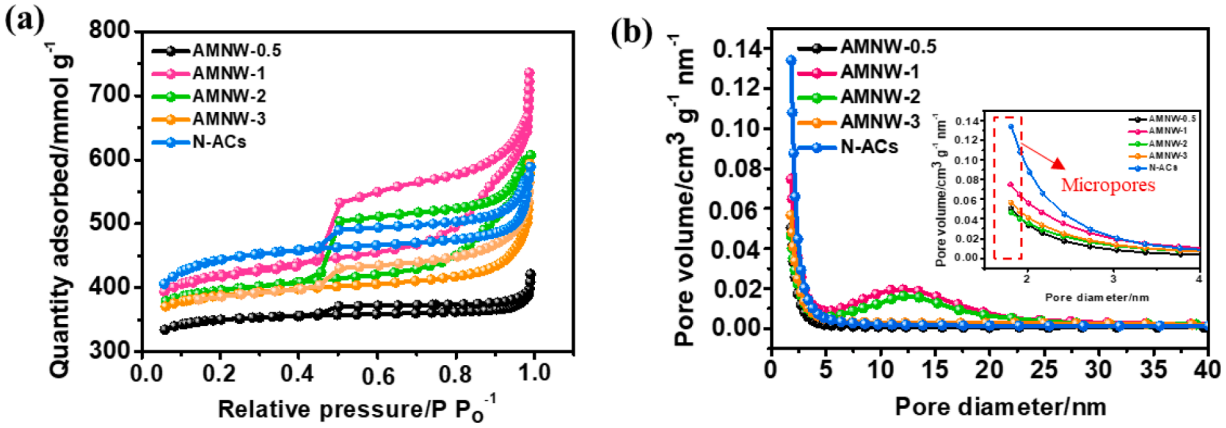


Fig. 3. (a) N_2 adsorption-desorption isotherm and (b) pore size distribution curves.

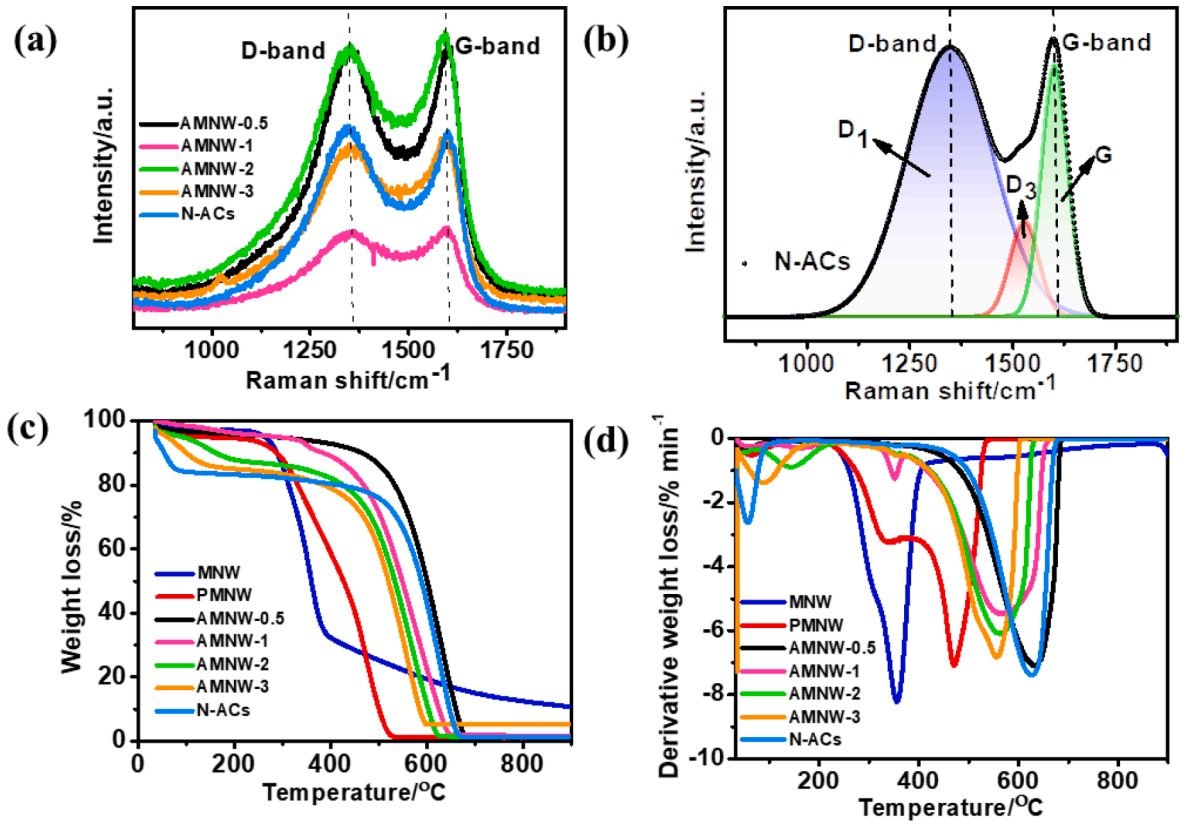


Fig. 4. (a) Raman spectra, (b) Deconvoluted Raman spectra of N-ACs, (c) TGA and (d) TGA-derivatives of activated carbons.

This mass loss is due to the reaction of KOH with the carbon Eqs. (8) and ((9)) [50,51]

$$6KOH + 2C \leftrightarrow 2K + 3H_2 + 2K_2CO_3 \quad (8)$$

$$K_2CO_3 + 2C \rightarrow 2K + 3CO \quad (9)$$

The reaction between carbon and KOH showed that when the impregnation ratio increased from 1:0.5 to 1:3, the % yield of carbon decreased (Fig. S1). This is in accordance with work reported by Marsh et al. [50] that the reaction between carbon and KOH lead to gasification of volatile matter from the carbon. Reaction between carbon and KOH follows Eqs. (6) and (7).

4.2. Morphology and surface area analysis

SEM images of the marula nuts before and after activation are shown in Fig. 2. The MNW sample (Fig. 2a) shows agglomerated nanoparticles with a smooth surface. After pre-treatment with 3% H_2SO_4 (Fig. 2b), the PMNW showed a morphology change compared to the MNW, and the production of a material with a rough surface. The pre-treatment was used to break down the lignin in the marula nuts and to allow access to the cellulose, and this reaction led to an increase in the surface area (Table S2) [52]. After activation of the four AMNM samples, SEM images showed that they all now contained irregular holes (AMNW-2 (Fig. 2c), AMNW-0.5 (Fig. S2a), AMNW-1 (Fig. S2b) and AMNW-3 (Fig. S2c). Such holes aid with the diffusion of the electrolyte ions during charge storage.

The textural properties of the activated carbons were determined and the N_2 adsorption-desorption data are shown in Fig. 3a and b. The adsorption-desorption isotherm of the activated materials all displayed a Type IV isotherm (Fig. 3a) according to the IUPAC classification with a H4 hysteresis loop [53,54]. The hysteresis loop was observed between the adsorption and desorption branches and indicates the presence of mesopores. A Type 1 isotherm was observed for MNW and PMNW (Fig. S3).

The surface area of the original material was close to zero $m^2\ g^{-1}$ and after pre-treatment (PMNW), this increased to 31 $m^2\ g^{-1}$ (Table S2). After activation, the surface area increased to between 1111 $m^2\ g^{-1}$ and 1353 $m^2\ g^{-1}$. While treatment of the PMNW with KOH, with the 1:1 AMNW:KOH ratio (AMNW-1), gave the ACs with the largest surface area, increasing the KOH ratio further did not increase the surface area. This indicates that as the impregnation ratio increased from 1 to 3 the excess KOH led to destruction of the carbon structure rather than creation of a more porous material. This is consistent with the decrease in total pore volume but minimal change in the micropore volume with variation of the KOH ratio (Table S2; Fig. 3b) [54].

4.3. Raman and TGA analysis

The Raman spectra of the materials are shown in Fig. 4a. The Raman spectra were used to evaluate the combined effect of activation and carbonization of the carbons. The Raman shift of all the materials showed the presence of a D-band (~1349 cm^{-1}) (called D_1 in the analysis; see below) and a G-band (~1598–1600 cm^{-1}) [55] (Table S3). The presence of the D-band is due to defects in the material and the G-band is a feature of the sp^2 graphitic materials [56]. The deconvoluted spectra of the activated materials also showed the presence of a further vibration (D_3; Fig. S4). The D_3 band result from amorphous carbon,and disordered graphitic lattice. The D_3 band is more visible in AMNW-2 and AMNW-3 due to higher concentration of KOH that led to destruction of the carbon. A measure of the disorder in the materials is given by the D_1/G band area ratios. As can be seen (Table S3), the disorder increased with the KOH: carbon ratio viz. 2.9 (AMNW-0.5) < 3.9 (AMNW-1) < 4.3 (AMNW-2) < 4.5 (AMNW-3).

Fig. 4c,d shows the TGA and TGA-derivative curves of the pristine, pretreated, and activated marula nuts. MNW (Fig. 4d) showed three weight losses at 52 °C [57], due to loss of moisture, at 295 °C, due to

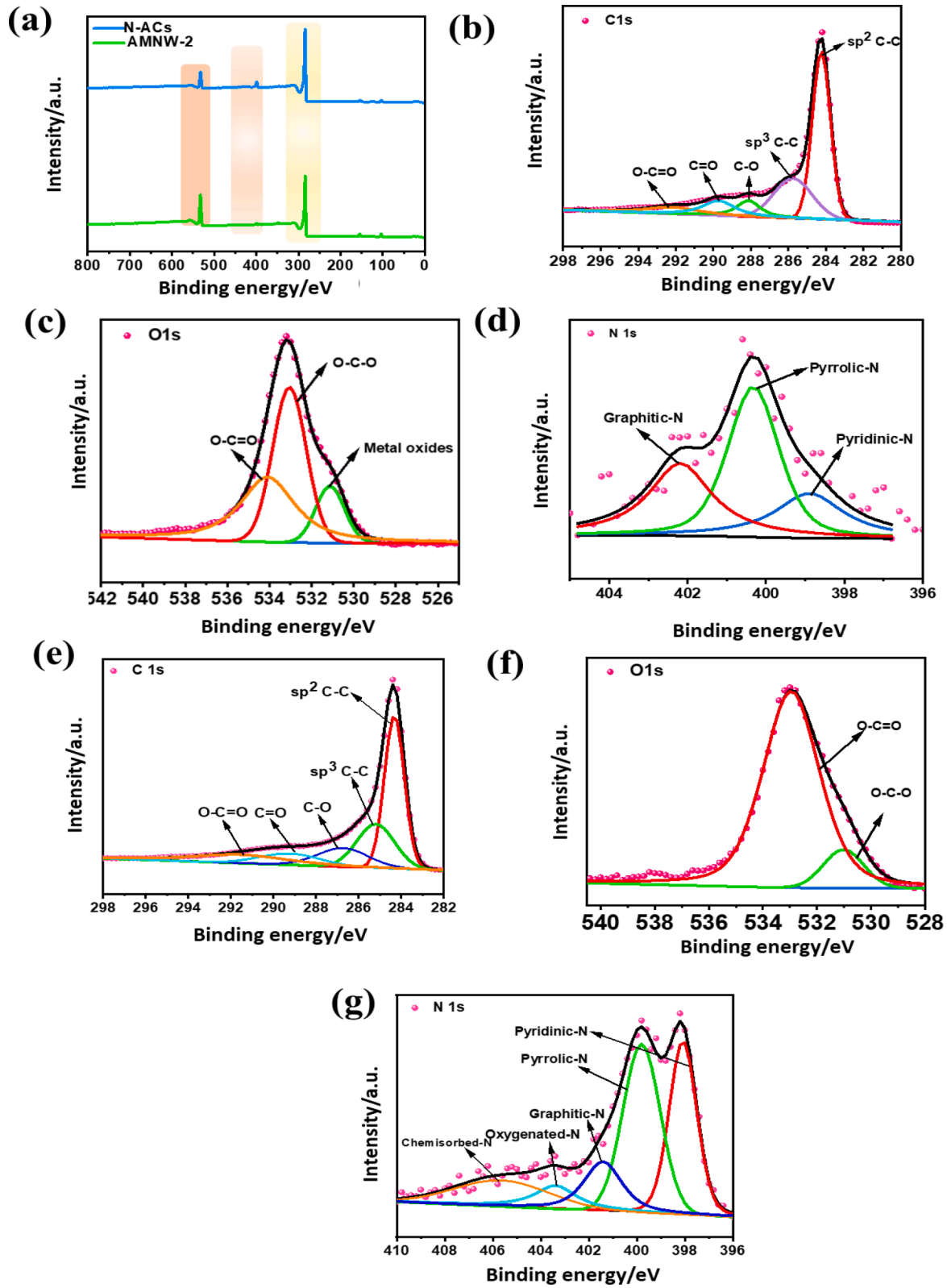


Fig. 5. (a) Survey scans of AMNW-2 and N-ACs, (b) C1s, (c) O1s and (d) N1s deconvoluted spectrum of AMNW-2, (e) C1s, (f) O1s and (g) N 1 s deconvoluted spectrum of N-ACs.

polymer (cellulose and hemicellulose) degradation [58] and at 356 °C due to lignin loss [58]. The remaining mass of MNW was 11% (Fig. 4c) showing the presence of inorganic compounds in the material. The PMNW showed a weight loss at ~63 °C due to the loss of moisture and two other degradation events at 337 and 471 °C due to the breakdown of lignin and removal of most of the inorganic material ca. 1% residue).

Activation with KOH resulted in removal of carbons that gave rise to the peak at ca. 400 °C and a shift (and broadening) of the major peak from 620 °C to ca. 550 °C with increasing KOH:carbon ratio. This is consistent with the formation of a more porous material with activation

Table 2
XPS atom % of AMNW-2 and N-ACs.

Type of material	XPS atom %		
	C	O	N
AMNW-2	78.3	16.8	0.9
N-ACs	84.9	7.9	5.1

[59]. The small peaks at 351 °C (AMNW-1) and 358 °C (AMNW-2 and AMNW-3) are due to the presence and degradation of lignin. The materials all showed small amounts (1 −5%) of residue which can be due to the ash content present in the materials.

4.4. Effect of nitrogen-doping on activated carbons

Nitrogen doping was only performed on the AMNW-2 as (i) it showed slightly high number of micropores area that facilitates charge storage and (ii) defects which can improve electron transport.

SEM images of the N-ACs is shown in Fig. 2d,e. The SEM image still clearly shows the presence of the irregular holes seen in the SEM image of AMNW-2. Energy dispersive spectroscopy (EDS) mapping was applied to investigate the elements present in the N-ACs. This also showed that the nitrogen was evenly dispersed across the carbon (Fig. 2g).

The surface area of AMNW-2 increased from 1266 to 1427 $m^2\ g^{-1}$ on N doping (Fig. 3a and Table S2). This surface area increase suggests that the melamine decomposition, that covers the surface with C and N atoms and does not cover the holes that were formed due to the KOH reaction with carbon [60].

The Raman spectra was recorded and the peaks deconvoluted using a Lorentzian function in order to calculate the area ratio of the D-band to the G-band (Fig. 4b). Upon introducing nitrogen to AMNW-2, the G-band shifted to a higher wavenumber (Table S3) and the D_1/G ratio decreased from 4.3 to 3.5. This observation suggests that even though the addition of N will produce a less graphitized carbon surface, the added annealing at the high temperature is a more important factor in determining the surface structure. The decrease of the D_1/G ratio is also influenced by the increase in the number of carbon atoms introduced from melamine resulting in the further graphitization of the material [60].

TGA was performed on the N-ACs sample. N-ACs was more thermally

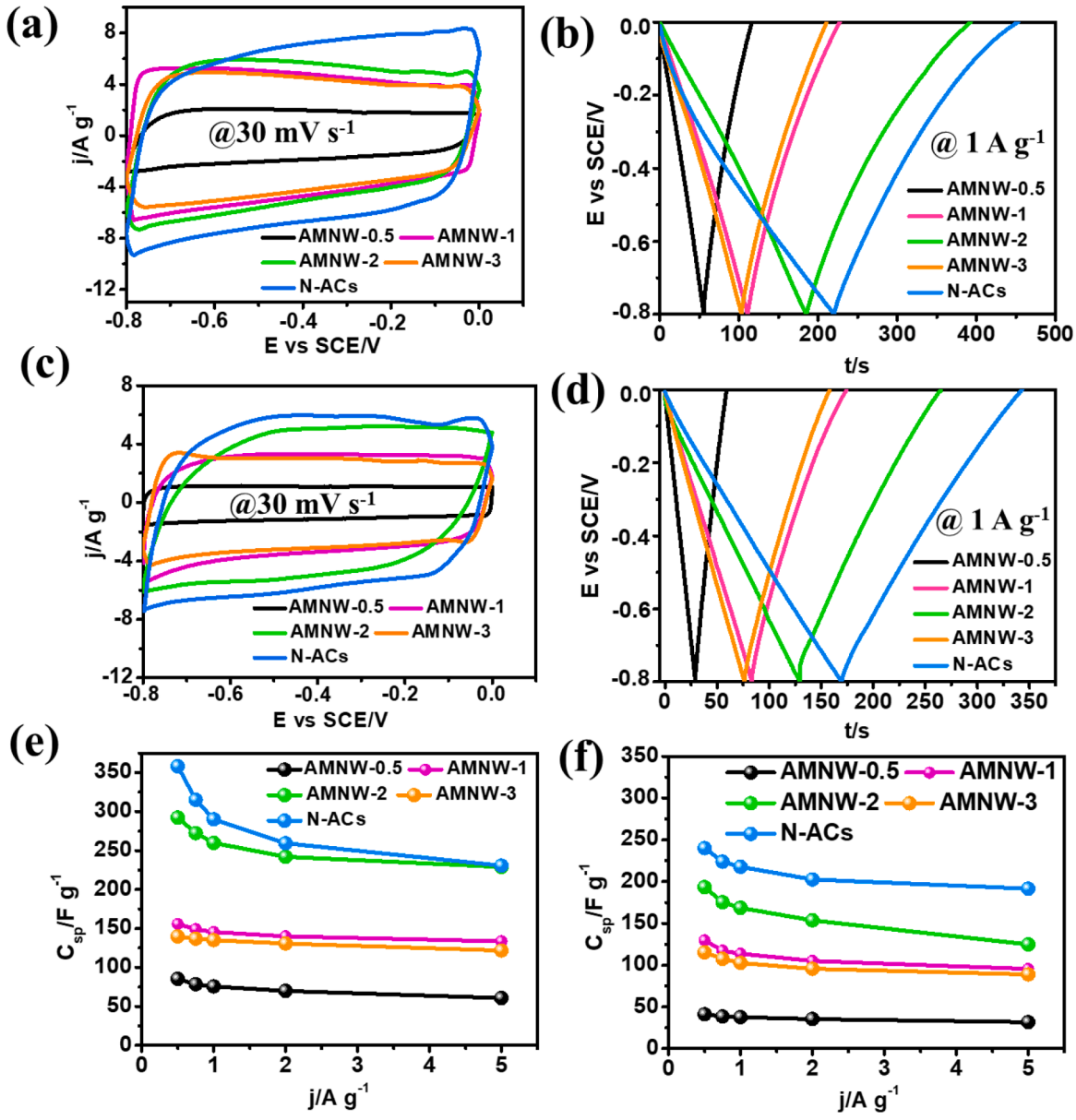


Fig. 6. (a) CV, (b) GCD, (e) Csp VS current density in 6 M KOH, (c) CV, (d) GCD, (e) and (f) Csp VS current density in 2.5 M KNO_3 of ACs and N-ACs.

stable than AMNW-2 with a carbon decomposition temperature at 630 °C (Fig. 4d) as compared to a temperature of 589 °C for the AMNW-2 material. The high stability of N-ACs might be due to the increase of carbon content from melamine decomposition (Fig. 4c).

4.5. XPS analysis

The survey XPS scan of N-ACs and AMNW-2 (Fig. 5a) showed the presence of C1s, N1s and O1s at ca. 284 eV, 399 eV and 532 eV [61]. The presence of N in AMNW-2 indicates that marula nuts waste naturally contains a small amount of nitrogen (0.9%) (Table 2). After nitrogen doping of AMNW-2, the nitrogen content of the N-ACs was found to be 5.1% (Table 2).

The C1s peak for AMNW-2 was deconvoluted, resulting in the detection of five different C atom types (Fig. 5b). The signals comprise of sp^2 C-C (284.2 eV), sp^3 C-C (285.8 eV), C-O (288.2 eV), C=O (289.8 eV) and O-C=O (292.4 eV) [62,63]. The O1s peak seen in the survey scan was also deconvoluted and is shown in Fig. 5c with metal oxides at 531.2 eV, O-C-O (533.1 eV) and O-C=O (534.1 eV) [64,65] The N1s peak deconvolution was done, and it showed three peaks which are attributed to pyridinic-N (398.8 eV), pyrrolic-N (399.8 eV) and graphitic-N (402.2 eV) (Fig. 5d) [66].

The C1s peak for N-ACs was deconvoluted (Fig. 5e) and it showed five carbon signals for sp^2 C-C/sp^2 C-N (284.2 eV), sp^3 C-C/sp^3 C-N (285.2 eV), C-O (286.8 eV), C=O (289.2 eV) and O-C=O/N-C=O (291.7 eV) [62]. The C1s peak for N-ACs showed a decrease of atomic % of C-C sp^2 (31.4%) and C-C sp^3 (18.9%) as compared to C-C sp^2 (52.7%) and C-C sp^3 (26.4%) for AMNW-2 (Table S4). This can be attributed to the formation of C-N bonds that are formed when nitrogen is introduced to the activated material. This shows that the decomposition of melamine generates more C-N bonds.

The deconvolution of O1s was also done and it comprises of two signals (Fig. 5f) at 531.2 eV and 533.0 eV for O-C-O and O-C=O [64,67]. As seen from Table S4, the atomic % of O-C=O oxygen decreased after nitrogen doping. This is due to the removal of oxygen on the surface after reaction with the melamine, to form nitrogen containing surface species. The deconvolution of the N-ACs N1s peak gave rise to five signals (Fig. 5g) [68]. The five signals comprises of pyridinic-N at 398.1 eV, pyrrolic-N at 399.6 eV, graphitic-N at 401.4 eV, oxygenated-N at 403.4 eV and chemisorbed-N at 405.8 eV [69,70]. As seen from Table S4, there are mainly pyridinic and pyrrolic species which are chemically active nitrogen bonding configurations enhancing the conductivity of the material, which is essential for improving capacitance. These results are in good agreement with the data reported by Guan et al. for nitrogen doping of activated carbon from pine nut shell using melamine as nitrogen source [71].

4.6. Electrochemical analysis

The electrochemical properties of the ACs were analysed in a three-electrode system using 6 M and 2.5 KNO_3 electrolyte in a potential range (E vs SCE/V) of −0.8–0.0 V as shown in Fig. 6. Fig. 6a,c shows the cyclic voltammograms (CV) of the materials at 30 mV s^{-1} in 6 M KOH (Fig. 6a) and 2.5 KNO_3 (Fig. 6c). All the CV curves have a rectangular shape demonstrating an electric double layer capacitance [72]. AMNW-2 showed a higher current response than the other ACs in both 6 M KOH and 2.5 M KNO_3. This was not directly related to surface area since AMNW-1 had the highest surface area (1353 m^2 g^{-1}). This is not unexpected since the surface area is not directly proportional to capacitance as capacitance depends on other factors such as conductivity, porosity and the type of electrolyte used [73]. AMNW-2 had the highest micropore volume and this could have been the important property that determined the current response that serve as charge storage as compared to mesopores which facilitates charge movement [74].

Fig. 6b, d shows the charge-discharge curves for activated carbons materials at 1 A g^{-1} and this figure displays a triangular shape which is characteristic of an ideal capacitor [75]. AMNW-2 displayed a higher discharge time than the other undoped activated carbons in both 6 M KOH and 2.5 M KNO_3.

Upon doping AMNW-2 with nitrogen, the current response improved in both 6 M and 2.5 KNO_3 due to an improved conductivity (see EIS data below). Comparing N-ACs in both 6 M KOH and 2.5 M KNO_3, the N-ACs had a high current response (Fig. 6a), a long discharge time (Fig. 6b), and a high specific capacitance (Fig. 6e) in 6 M KOH than in 2.5 M KNO_3. N-ACs performed better in 6 M KOH than in 2.5 KNO_3.

The calculated capacitance of all the materials are listed in Table S5. Table S5 shows that increasing current densities leads to limited amount of charge stored hence the decrease in capacitance (Fig. 6e,f).

The high capacitance of the materials in 6 M KOH than in 2.5 M KNO_3 is attributed to the high ionic conductivity of the KOH electrolyte. According to previous studies [76,77], the excellent electrochemical performance of carbon materials in 6 M KOH can be due to ionic mobility, conductivity, and electrolyte pH. Table 3 summarizes the parameters of the electrolytes showing that KOH have higher conductivity and high ionic mobility hence the higher capacitances. Again, the high amount of charge stored in N-ACs can be attributed to an improved conductivity [78]. Wang et al. [79] also reported an increase in capacitance due to the influence of nitrogen on activated carbons, implying that nitrogen doping improved the conductivity of the material.

The high conductivity (198 Scm^2 mol^{-1}) and smaller hydrated size (3.00 Å) of OH^- ions compared to NO^{3-} ions explains why KOH has a higher ion mobility and conductivity than NO^{3-} [39]. Hence, the high capacitance values of the materials when using KOH electrolyte.

However, operating the cell in a wider voltage in 6 M KOH is limited due to the water decomposition at 1.23 V [78]. When compared to alkaline electrolytes (i.e. KOH), neutral electrolytes (i.e. KNO_3) can be operated at a high voltage (~2 V) because the H^- and OH^- concentrations are lower, resulting in a potential shift of the hydrogen and oxygen evolution to a wider stable potential window, that increases the amount of energy stored. For example, Sheng et al. reported on the use of a 1 M Na_2SO_4 neutral electrolyte with an operating voltage up to 1.6 V giving an energy density of 25.7 Wh kg^{-1} [78]. Neutral electrolytes have been reported to have a higher voltage window and to be less corrosive than alkaline electrolytes [80]. As a result, carbon-based materials in symmetric devices using neutral electrolytes have been considered as a possible way to achieve higher energy density while reducing the impact of corrosive effects on the device. Hence, in this study, a symmetric device was assembled and operated at a wider potential using 2.5 M KNO_3 to enhance the energy density.

Due to the wide potential window of the neutral electrolyte, N-ACs was run at different cell potential from 1.5–2.0 V as shown from CV curves (Fig. 7a) and GCD curves (Fig. 7b) in 2.5 M KNO_3 electrolyte. Both CV and GCD curves show that the cell potential becomes stable up to 1.8 V and further increasing the potential up to 2 V changes the CV and GCD shape due to the polarization of the material as the electrolyte decomposes at high potential range (> 1.8 V). Hence, the material was further run at different scan rates and current densities at a cell potential of 1.8 V. The cell potential of neutral electrolytes can reach up to 1.8 V due to the low concentrations of H^+ and OH^-, given that increased oxygen and dihydrogen evolution increases the electrolyte stability window [81]. The wider stability window of neutral electrolytes can be explained by the high overpotential as effects of ion hydration fundamentals processes [82–84]. This is due to the fact that neutral

Table 3
Summary of the sizes of ions [39].

Type of ion	Size of bare ion/Å	Size of hydrated ion/Å	Ionic conductivity/Scm^2 mol^{-1}
K^+	1.15	3.31	73.5
OH^-	1.76	3.00	198
NO^{3-}	2.64	3.35	71.42

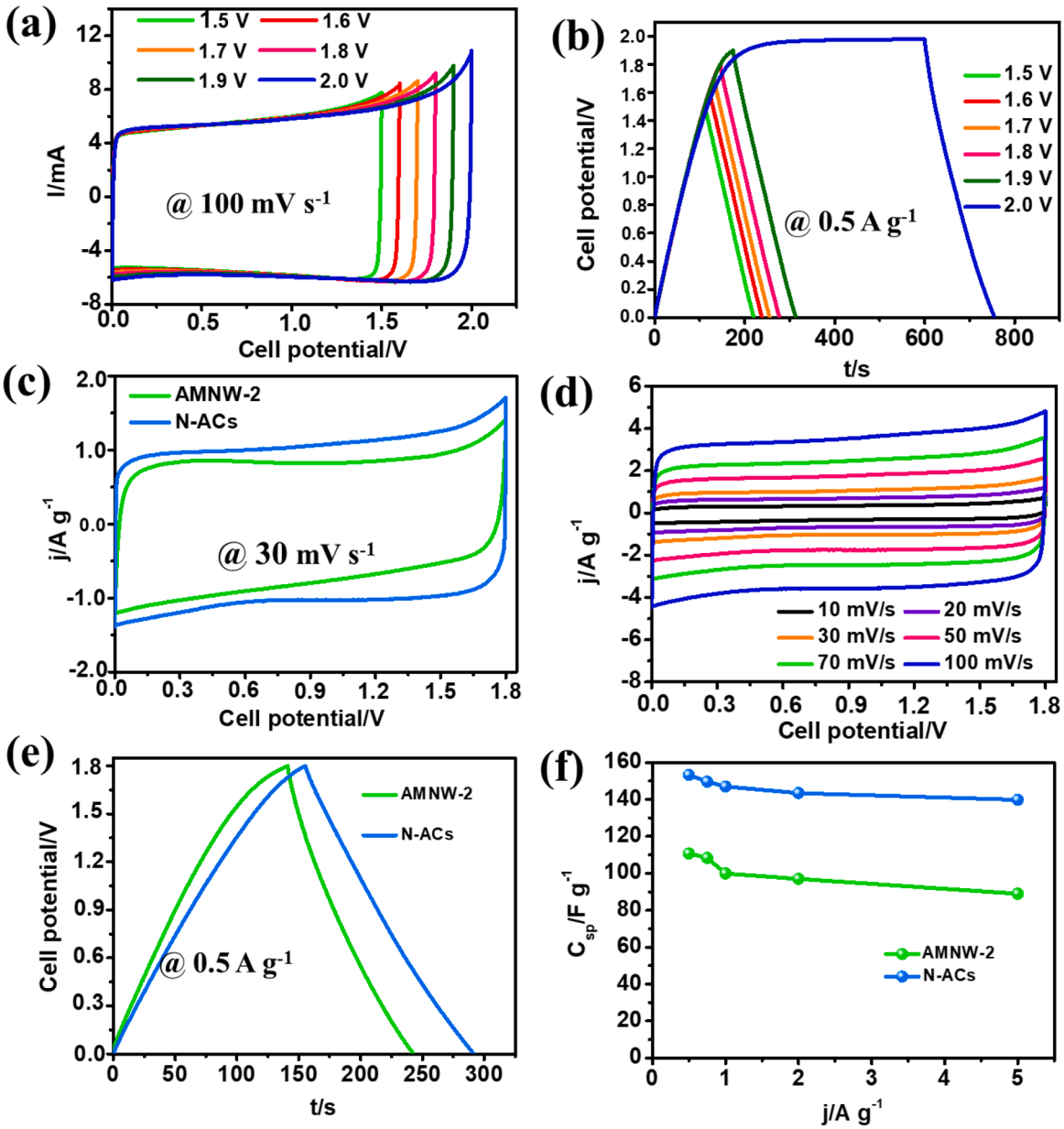


Fig. 7. (a) CV tests of N-ACs at different cell potential (b) GCD curves of N-ACs at different cell potential, (c) CV curves comparison of AMNW-2 and N-ACs at 30 mV s^{-1}, (d) CV curves of N-ACs at different scan rates, (e) GCD and (e) specific capacitance comparison of AMNW-2 and N-ACs current densities in 2.5 M KNO_3.

electrolytes lack free H^+ and OH^-resulting in high overpotential on both hydrogen evolution reaction (HER) and oxygen evolution reaction (OER). This notion was used by Hong et al. by comparing linear weep voltammetry of 1 M HCl, KOH, and KCl, where the water electrolysis happening in KCl had similar onset potentials as the OER in HCl to HER in KOH solutions [83]. This perception implied that HER and OER occurred through direct oxidation/reduction of water molecules [85] the amount of reactant for water decomposition can be depleted by reducing the concentration of water which further widen the electrochemical stability.

The CV curves of AMNW-2 and N-ACs were then compared at 30 mV s^{-1} (see Fig. 7c). N-ACs showed a high current response which can be attributed to the higher conductivity of the material arising from the high nitrogen content of 5.1% [86]. CV curves of N-ACs were ran at different scan rates from (Fig. 7d) and showed the rectangular shape of an ideal capacitor. GCD curves of the materials (Fig. 7e) were compared at 0.5 A g^{-1} and they showed a triangular shape which is that of an ideal capacitor. N-ACs showed a higher charge-discharge time which is in good agreement with the high current from the CV curves. The GCD curves of N-ACs were ran at current densities from 0.5–5 A g^{-1} (Fig. S5) and showed a triangular shape which is that of an ideal capacitor indicating reversible adsorption and desorption of electrolyte ions.

The specific capacitance was calculated from these GCD curves using Eq. (4) and the capacitance decreased as the current density increased which indicates a good rate capability (Fig. 7f). The capacitance of N-ACs obtained at 0.5 A g^{-1} was 153.3 F g^{-1} and 139.8 F g^{-1} at 5 A g^{-1}.

The Nyquist plots (Fig. 8a) of AMNW-2 and N-ACs were modelled before and after 6 000 cycles. The material's bulk properties were shown by the presence of the bulk resistance (R_s) (i.e. electrodes, electrolytes, current collectors and separators), charge transfer resistance (R_{ct}), internal resistance (R_{int}), double layer capacitance (Cd_{ll}) and the constant phase element (CPE) due to the materials porosity [87,88] The impedance power law relationship of CPE (ZCPE) is shown in Eq. (10):

$$Z_{CPE} = [Q(j\omega)^n]^{-1} \quad (10)$$

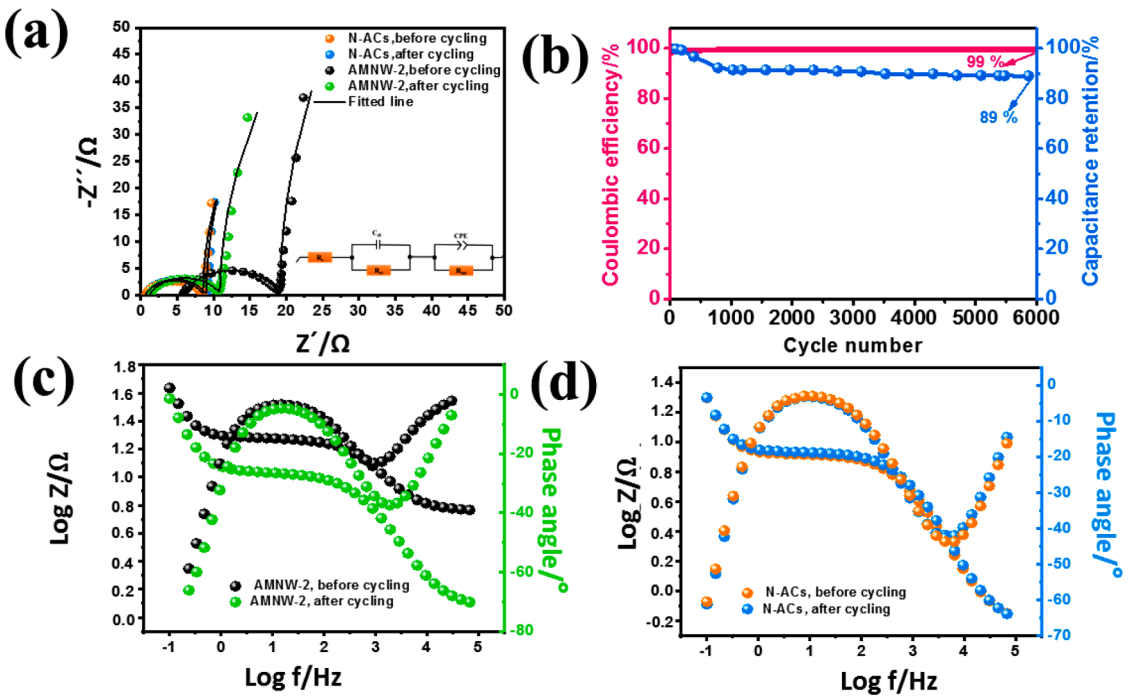


Fig. 8. (a) Nyquist plots of AMNW-2 and N-ACs obtained before and after 6000 cycles with electrical equivalent circuit used to fit Nyquist plots, (b) cyclic stability of N-ACs and (c,d) Bode plots before and after 6000 cycles of the AMNW-2 and N-ACs symmetric cells.

Table 4
EIS parameters of the synthesized materials for two-electrode system in 2.5 M KNO_3.

EIS parameters	Electrode material for the symmetric supercapacitor			
	AMNW-2		N-ACs	
	Before cycling (1st cycle)	After cycling (6,000th cycle)	Before cycling (1st cycle)	After cycling (6,000th cycle)
R_s / Ω	5.70 ± 0.47	1.18± 0.47	0.60 ± 0.46	0.59 ± 0.47
ESR (R_{ct}) / Ω	13.48 ± 0.82	9.77 ± 0.84	8.44 ± 0.79	7.99 ± 0.81
C_{dl} / μF	41.26 ± 3.61	45.54 ± 4.45	89.19 ± 0.02	90.67 ± 0.02
R_{int} / Ω	344.70 ± 277.10	235.3 ± 158.1	224.3 ± 558.6	186.01 ± 384.0
CPE /mF $s^{\wedge(a-1)}$	0.13 ± 0.11	0.21 ± 0.28	0.15 ± 0.24	0.17 ± 0.30
N	0.77	0.76	0.79	0.77
f_o / Hz	11.4	16.9	25.1	25.1
τ / ms	88	59	40	40
Phase angle	59°	66°	61°	60°

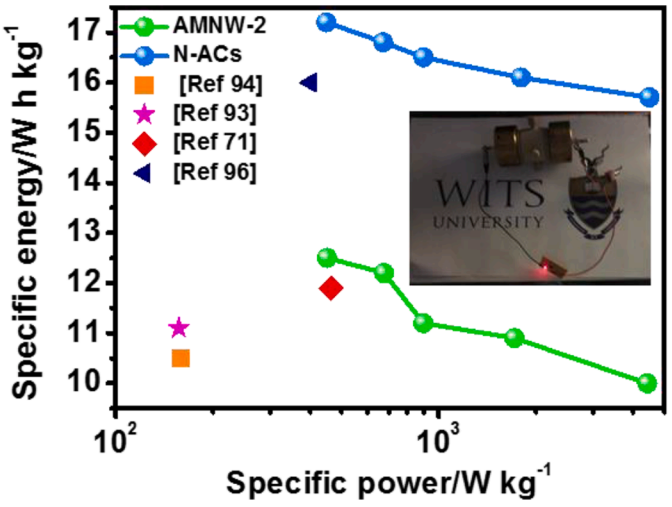


Fig. 9. Ragone plot of AMNW-2 and N-ACs. The inset shows an image of a red LED powered by the N-ACs electrode-based device.

where Q represents the frequency-independent constant, $j = \sqrt{-1}$, radial frequency is represented by symbol ω, and n lies between −1 and 1 ($-1 \leq n \leq 1$) which is the slope of Log Z vs. Log *f*.

The CPE becomes a pure resistor when $n = 0$, while the CPE is that of a pure capacitor when $n = 1$, and when $n=-1$, the CPE is that of an inductor. However, when $n = 0.5$, the CPE can be regarded as equivalent to a Warburg impedance (Z_w) [47]. From Table 4, the value of $n = 0.77$ for N-ACs after cycling demonstrates the nature of N-ACs as an EDCLs material.

The R_s value of N-ACs is 0.59 Ω, which is lower than the R_s value of AMNW-2 (1.18 Ω) after cycling and suggests that nitrogen improved the solution resistance of the ACs. The R_{CT} value of the N-ACs was also smaller (7.99 Ω) than that of the AMNW-2 (9.77 Ω), which is due to the improved conductivity resulting in better electrode/electrolyte surface contact from the nitrogen doping [89,90]. Interestingly, the Cd_{ll} for N-ACs was higher before and after cycling than AMNW-2 which indicates that nitrogen doping made the carbon materials more capacitive. The R_{int} obtained for N-ACs after cycling was smaller (~ 186 Ω) than AMNW-2 (~235 Ω). Given that R_{int} is mainly due to the ohmic drop (IR drop) and diffusion rate of electrolytes ions [91], hence N-ACs gave a smaller R_{int} than AMNW-2 due to the improved surface contact of the material and electrolytes ions. The knee frequency (f_o / Hz) from the EIS data (Table 4) was estimated and gave the power capability of the materials. A high value of the f_o / Hz indicates the capability of a material to have a high power density and to provide energy density in a short time frame. The EIS parameters in Table 4 show that N-ACs gave a higher f_o (ca. 25.1 Hz, response time, τ of 40 ms) after 6000th cycles. This is important if one considers that high powered supercapacitors available commercially operate at less than 1 Hz. The phase angles of the symmetric cells after cycling, as determined by Bode plots (Fig. 8c & d), demonstrated that the AMNW-2 symmetric cell (69°) cell has a higher

Table 5
Summary of energy and power densities of activated carbons in SCs.

Biomass	Precursor	Surface area (m^2 g^{-1})	Electrolyte	Cell potential (V)	Current density (A g^{-1})	Specific energy (W h kg^{-1})	Specific power (W kg^{-1})	Reference
Activated carbons								
Marula nuts shell	KOH	1266	2.5 M KNO_3	2.0	0.5	12.5	451.4	This study
Hazel nutshell	MgO	552	1 M Na_2SO_4	2.0	0.25	11.1	156.8	[13]
Eucalyptus bark	KOH	1003	1 M Na_2SO_4	1.8	0.2	10.5	159.5	[92]
Cotton fibre	$ZnCl_2$	2549	1 M Na_2SO_4	1.8	0.5	13.75	–	[93]
		Nitrogen doping						
N-ACs	KOH/ melamine	1427	2.5 M KNO_3	2.0	0.5	17.2	448.7	This study
Pine nut shells	KOH/ melamine	1806	1 M $NaSO_4$	1.8	1.0	11.9	463.6	[71]
Orange peel	$FeCl_3$/Urea	1514.2	0.5 M Li_2SO_4	1.6	0.5	16	400	[94]
Cellulose	NaOH/urea	2245	1 M Na_2SO_4	1.8	0.5	17.24	452	[95]

phase angle at low frequencies, implying decreased ionic permeability and thus insulating characteristics. The high ionic permeability of the N-ACs symmetric cell (60°) cell occurs at low frequencies, which is indicative of poor insulation, revealing that the N-ACs electrode material is permeable to solution ions.

The cyclic stability of N-ACs for the symmetric device was tested using charge-discharge up to 6000 cycles at a current density of 5 A/g (Fig. 8b). A Coulombic efficiency of 99% was obtained with a capacitance retention of 89%. The excellent capacitance retention of the material is due to its structural stability that permits the re-usability of the material.

The evaluation of the amount of charge stored and the rate at which it was delivered can be determined by two parameters: energy and power density. A Ragone plot of the materials is shown in Fig. 9. The N-ACs demonstrated a higher energy density of 17.2 Wh kg^{-1} and a power density of 448.7 W kg^{-1}, than that of AMNW-2 (12.5 Wh kg^{-1}). The improved energy density of N-ACs is due to the improved conductivity and total surface area of the material. The energy density of ACs from marula nuts waste in this study is comparable to activated carbons from hazel nutshell with an energy density of 11.1 Wh kg^{-1} in 1.0 M Na_2SO_4 electrolyte [13]. In addition, the single device was connected to a light emitting diode (LED, 1.6 V) and this device successfully lit up a red LED (see inset in Fig. 9) for over a minute after charging for 20 s.

Our results indicate that nitrogen improves the specific capacitance of carbon. To place these current findings into perspective, the findings on activated carbons and nitrogen-doped activated carbons from the use of biomass in SCs, as well as their energy densities, is given in Table 5. The specific energy and power obtained in this study was comparable to other studies and in some cases found to be higher to other undoped porous carbons and nitrogen doped porous carbons. These results show that energy density depends on many factors such as activating agent, surface area, type of electrolyte, etc.

5. Conclusions

Nitrogen-doped activated carbons with a high porous surface area of 1427 m^2 g^{-1} and high nitrogen content of 5.1% was successfully synthesized from marula nuts via KOH activation and carbonization at 800 °C using melamine as a nitrogen source. Electrochemical characterizations of the materials were tested for supercapacitor applications using 6 M KOH and 2.5 M KNO_3 in three electrode system. AMNW-2 and N-ACs performed better in 6 M KOH than 2.5 M KNO_3 than the other activated materials due to the higher conductivity of the alkaline electrolyte. For a two-electrode system, the AMNW-2 and N-ACs were examined using 2.5 M KNO_3 with a wider cell voltage window of 1.8 V. The activated material gave an energy density of 12.5 Wh kg^{-1} which improved to 17.2 Wh kg^{-1} after doping with nitrogen. These results in a neutral 2.5 M KNO_3 electrolyte are fascinating, empowering, and demonstrate the feasibility of using marula nut waste to produce porous carbons, demonstrating the exciting potential for producing activated carbons at low cost, which could pique industry interest for possible application in energy storage.

CRediT authorship contribution statement

B. Shaku: Conceptualization, Methodology, Investigation, Validation, Writing – original draft. **T.P. Mofokeng:** Data curation, Methodology, Writing – review & editing. **N.J. Coville:** Resources, Writing – review & editing, Supervision. **K.I. Ozoemena:** Conceptualization, Supervision, Resources, Writing – review & editing. **M.S. Maubane-Nkadimeng:** Conceptualization, Supervision, Resources, Writing – review & editing.

Declaration of Competing Interest

The authors declare no known competing financial interests or personal relationships that could have influenced the work reported in this paper.

Data availability

Supplementary data for the manuscript is provided.

Acknowledgements

This work is supported by National Research Foundation (NRF) of South Africa (Grant Number: 138075), the University of the Witwatersrand and the Department of Science and Innovation (DSI-NRF) Centre of Excellence in Strong Materials. We acknowledge the financial support of the DSI-NRF-Wits SARChI Chair in Materials Electrochemistry and Energy Technologies (MEET) (UID No.: 132739).

Supplementary materials

Supplementary material associated with this article can be found, in the online version, at doi:10.1016/j.electacta.2023.141828.

References

[1] M.U. Sasmaz, E. Sakar, Y.E. Yayla, U. Akkucuk, The relationship between renewable energy and human development in OECD countries: a panel data analysis, Sustainability (Switzerland) 12 (2020) 1–16.
[2] Y. Li, X. Han, T. Yi, Y. He, X. Li, Review and prospect of NiCo2O4-based composite materials for supercapacitor electrodes, J. Energy Chem. 31 (2019) 54–78.
[3] Q. Geng, H. Wang, J. Wang, J. Hong, W. Sun, Y. Wu, Y. Wang, Boosting the capacity of aqueous Li-ion capacitors via pinpoint surgery in nanocoral-like covalent organic frameworks, Small Method. 6 (2022).
[4] C. Cai, Y. Zou, C. Xiang, H. Chu, S. Qiu, Q. Sui, F. Xu, L. Sun, A. Shah, Broccoli-like porous carbon nitride from ZIF-8 and melamine for high performance supercapacitors, Appl. Surf. Sci. 440 (2018) 47–54.
[5] F.W. Richey, C. Tran, V. Kalra, Y.A. Elabd, Ionic liquid dynamics in nanoporous carbon nanofibers in supercapacitors measured with in operando infrared spectroelectrochemistry, J. Phys. Chem. C 118 (2014) 21846–21855.
[6] Q. Wang, J. Yan, Y. Wang, T. Wei, M. Zhang, X. Jing, Z. Fan, Three-dimensional flower-like and hierarchical porous carbon materials as high-rate performance electrodes for supercapacitors, Carbon N Y 67 (2014) 119–127.
[7] Z.S. Wu, K. Parvez, X. Feng, K. Müllen, Graphene-based in-plane micro-supercapacitors with high power and energy densities, Nat. Commun. 4 (2013).
[8] M. Passalacqua, D. Lanzarotto, M. Repetto, M. Marchesoni, Advantages of using supercapacitors and silicon carbide on hybrid vehicle series architecture, Energies (Basel) 10 (2017) 1–14.
[9] D. Pech, M. Brunet, H. Durou, P. Huang, V. Mochalin, Y. Gogotsi, P.L. Taberna, P. Simon, Ultrahigh-power micrometre-sized supercapacitors based on onion-like carbon, Nat. Nanotechnol. 5 (2010) 651–654.
[10] M. Olivares-Marín, J.A. Fernández, M.J. Lázaro, C. Fernández-González, A. Macías-García, V. Gómez-Serrano, F. Stoeckli, T.A. Centeno, Cherry stones as precursor of activated carbons for supercapacitors, Mater. Chem. Phys. 114 (2009) 323–327.
[11] X. Zhu, S. Yu, K. Xu, Y. Zhang, L. Zhang, G. Lou, Y. Wu, E. Zhu, H. Chen, Z. Shen, B. Bao, S. Fu, Sustainable activated carbons from dead ginkgo leaves for supercapacitor electrode active materials, Chem. Eng. Sci. 181 (2018) 36–45.
[12] C. Peng, J. Lang, S. Xu, X. Wang, Oxygen-enriched activated carbons from pomelo peel in high energy density supercapacitors, RSC Adv. 4 (2014) 54662–54667.
[13] N. Sinan, E. Unur, Hydrothermal conversion of lignocellulosic biomass into high-value energy storage materials, J. Energy Chem. 26 (2017) 783–789.
[14] S. Shackleton, Livelihood benefits from the local level commercialization of savanna resources: a case study of the new and expanding trade in marula (Sclerocarya birrea) beer in Bushbuckridge, South Africa, S. Afr. J. Sci. 100 (2004) 651–657.
[15] C. Shackleton, S. Shackleton, The importance of non-timber forest products in rural livelihood security and as safety nets: a review of evidence from South Africa, S. Afr. J. Sci. 100 (2004) 658–664.
[16] T. Mkungunugwa, S. Manhokwe, A. Chawafambira, M. Shumba, Synthesis and characterisation of activated carbon obtained from marula (Sclerocarya birrea) nutshell, J. Chem. (2021) 2021.
[17] Q. Chen, X. Tan, Y. Liu, S. Liu, M. Li, Y. Gu, P. Zhang, S. Ye, Z. Yang, Y. Yang, Biomass-derived porous graphitic carbon materials for energy and environmental applications, J. Mater. Chem. A Mater. 8 (2020) 5773–5811.
[18] A. Javier Sánchez, Characterization of activated carbon produced from coffee residues by chemical and physical activation, KTH Chem. Sci. Eng. (2011) 66.
[19] A.S. Alzaydien, Physical, chemical and adsorptive characteristics of local oak sawdust based activated carbons, Asian J. Sci. Res. 9 (2016) 45–56.
[20] W. Li, L. bo Zhang, J. hui Peng, N. Li, X. yun Zhu, Preparation of high surface area activated carbons from tobacco stems with K2CO3 activation using microwave radiation, Ind. Crops Prod. 27 (2008) 341–347.
[21] J. Pallarés, A. González-Cencerrado, I. Arauzo, Production and characterization of activated carbon from barley straw by physical activation with carbon dioxide and steam, Biomass Bioenergy 115 (2018) 64–73.
[22] G. Lota, T.A. Centeno, E. Frackowiak, F. Stoeckli, Improvement of the structural and chemical properties of a commercial activated carbon for its application in electrochemical capacitors, Electrochim. Acta 53 (2008) 2210–2216.
[23] V. Ruiz, C. Blanco, E. Raymundo-Piñero, V. Khomenko, F. Béguin, R. Santamaría, Effects of thermal treatment of activated carbon on the electrochemical behaviour in supercapacitors, Electrochim. Acta 52 (2007) 4969–4973.
[24] B. Fang, Y.Z. Wei, M. Kumagai, Modified carbon materials for high-rate EDLCs application, J. Power Source. 155 (2006) 487–491.
[25] J. ichi Ozaki, N. Kimura, T. Anahara, A. Oya, Preparation and oxygen reduction activity of BN-doped carbons, Carbon N Y 45 (2007) 1847–1853.
[26] X. Yan, Y. Jia, X. Yao, Defects on carbons for electrocatalytic oxygen reduction, Chem. Soc. Rev. 47 (2018) 7628–7658.
[27] W. Han, H. Wang, K. Xia, S. Chen, P. Yan, T. Deng, W. Zhu, Superior nitrogen-doped activated carbon materials for water cleaning and energy storing prepared from renewable leather wastes, Environ. Int. 142 (2020), 105846.
[28] B. Li, F. Dai, Q. Xiao, L. Yang, J. Shen, C. Zhang, M. Cai, Nitrogen-doped activated carbon for a high energy hybrid supercapacitor, Energy Environ. Sci. 9 (2016) 102–106.
[29] X. Wang, Y. Liu, L. Zhu, Y. Li, K. Wang, K. Qiu, N. Tippayawong, P. Aggarangsi, P. Reubroycharoen, S. Wang, Biomass derived N-doped biochar as efficient catalyst supports for CO2 methanation, J. CO2 Utilizat. 34 (2019) 733–741.
[30] Y. Ding, Y. Li, Y. Dai, X. Han, B. Xing, L. Zhu, K. Qiu, S. Wang, A novel approach for preparing in-situ nitrogen doped carbon via pyrolysis of bean pulp for supercapacitors, Energy 216 (2021), 119227.
[31] S. Ahmed, M. Rafat, A. Ahmed, Nitrogen doped activated carbon derived from orange peel for supercapacitor application, Adv. Nat. Sci.: Nanosci. Nanotechnol. 9 (2018).
[32] M. Sevilla, G.A. Ferrero, N. Diez, A.B. Fuertes, One-step synthesis of ultra-high surface area nanoporous carbons and their application for electrochemical energy storage, Carbon N Y 131 (2018) 193–200.
[33] M. Zhou, F. Pu, Z. Wang, S. Guan, Nitrogen-doped porous carbons through KOH activation with superior performance in supercapacitors, Carbon N Y 68 (2014) 185–194.
[34] R.J. Mo, Y. Zhao, M. Wu, H.M. Xiao, S. Kuga, Y. Huang, J.P. Li, S.Y. Fu, Activated carbon from nitrogen rich watermelon rind for high-performance supercapacitors, RSC Adv. 6 (2016) 59333–59342.
[35] K. Kierzek, G. Gryglewicz, Activated carbons and their evaluation in electric double layer capacitors, Molecules 25 (2020).
[36] A. Lewandowski, A. Olejniczak, M. Galinski, I. Stepniak, Performance of carbon-carbon supercapacitors based on organic, aqueous and ionic liquid electrolytes, J. Power Source. 195 (2010) 5814–5819.
[37] F. Béguin, V. Presser, A. Balducci, E. Frackowiak, Carbons and electrolytes for advanced supercapacitors, Adv. Mater. 26 (2014) 2219–2251.
[38] H. Jiang, Y. Tian, M. Liu, X. Zhou, R. Xue, Influence of KNO3 on capacitive properties of active carbon in potassium ferricyanide solutions, Int. J. Electrochem. Sci. 17 (2022) 1–12.
[39] C. Zhong, Y. Deng, W. Hu, J. Qiao, L. Zhang, J. Zhang, A review of electrolyte materials and compositions for electrochemical supercapacitors, Chem. Soc. Rev. 44 (2015) 7484–7539.
[40] C.L. Lee, K.L. Chin, P.S. H'ng, U. Rashid, M. Maminski, P.S. Khoo, Effect of pretreatment conditions on the chemical–structural characteristics of coconut and palm kernel shell: a potentially valuable precursor for eco-efficient activated carbon production, Environ. Technol. Innov. 21 (2021).
[41] Y. Guo, Z. Zeng, Y. Liu, Z. Huang, Y. Cui, J. Yang, One-pot synthesis of sulfur doped activated carbon as a superior metal-free catalyst for the adsorption and catalytic oxidation of aqueous organics, J. Mater. Chem. A Mater. 6 (2018) 4055–4067.
[42] L. Chen, T. Ji, L. Mu, J. Zhu, Cotton fabric derived hierarchically porous carbon and nitrogen doping for sustainable capacitor electrode, Carbon N Y 111 (2017) 839–848.
[43] E. Zhen, J. Jiang, C. Lv, X. Huang, H. Xu, H. Dou, X. Zhang, Effects of binder content on low-cost solvent-free electrodes made by dry-spraying manufacturing for lithium-ion batteries, J. Power Source. 515 (2021).
[44] W. Yang, Z. Gao, J. Wang, J. Ma, M. Zhang, L. Liu, Solvothermal one-step synthesis of Ni-Al layered double hydroxide/carbon nanotube/reduced graphene oxide sheet ternary nanocomposite with ultrahigh capacitance for supercapacitors, ACS Appl. Mater. Interface. 5 (2013) 5443–5454.
[45] W. Sun, Y. Zhang, F. Yang, Tuning electrochemical performance of carbon-sphere-based supercapacitors by compressive stress, Electrochim. Acta 357 (2020).
[46] K. Makgopa, P.M. Ejikeme, C.J. Jafta, K. Raju, M. Zeiger, V. Presser, K. I. Ozoemena, A high-rate aqueous symmetric pseudocapacitor based on highly graphitized onion-like carbon/birnessite-type manganese oxide nanohybrids, J. Mater. Chem. A Mater. 3 (2015) 3480–3490.
[47] T.P. Mofokeng, Z.N. Tetana, K.I. Ozoemena, Defective 3D nitrogen-doped carbon nanotube-carbon fibre networks for high-performance supercapacitor: transformative role of nitrogen-doping from surface-confined to diffusive kinetics, Carbon N Y 169 (2020) 312–326.
[48] K. Makgopa, P.M. Ejikeme, K.I. Ozoemena, Graphene oxide-modified nickel (II) tetra-aminophthalocyanine nanocomposites for high-power symmetric pseudocapacitor, Electrochim. Acta 212 (2016) 876–882.
[49] H.M. Yang, D.H. Zhang, Y. Chen, M.J. Ran, J.C. Gu, Study on the application of KOH to produce activated carbon to realize the utilization of distiller's grains, IOP Conf. Ser. Earth Environ. Sci. 69 (2017).
[50] Harry. Marsh, F. Rodríguez-Reinoso, Activated Carbon, Elsevier, 2006.
[51] J. Andas, M.L.A. Rahman, M.S.M. Yahya, Preparation and characterization of activated carbon from palm kernel shell, in: IOP Conf Ser Mater Sci Eng, Institute of Physics Publishing, 2017.
[52] G. Brodeur, E. Yau, K. Badal, J. Collier, K.B. Ramachandran, S. Ramakrishnan, Chemical and physicochemical pretreatment of lignocellulosic biomass: a review, Enzyme Res. 2011 (2011).
[53] W. Zhou, S. Lei, S. Sun, X. Ou, Q. Fu, Y. Xu, Y. Xiao, B. Cheng, From weed to multi-heteroatom-doped honeycomb-like porous carbon for advanced supercapacitors: a gelatinization-controlled one-step carbonization, J. Power Source. 402 (2018) 203–212.
[54] K. Dujearic-Stephane, M. Gupta, A. Kumar, V. Sharma, S. Pandit, P. Bocchetta, Y. Kumar, The effect of modifications of activated carbon materials on the capacitive performance: surface, microstructure, and wettability, J. Composit. Sci. 5 (2021) 1–26.
[55] Y. Wang, D.C. Alsmeyer, R.L. McCreery, Raman spectroscopy of carbon materials: structural basis of observed spectra, Chem. Mater. 2 (1990) 557–563.
[56] J.R. Dennison, M. Holtz, Raman spectroscopy of carbon materials, Spectroscopy (Santa Monica) 11 (1996) 38–46.
[57] J.N. Edokpayi, S.S. Ndlovu, J.O. Odiyo, Characterization of pulverized marula seed husk and its potential for the sequestration of methylene blue from aqueous solution, BMC Chem. 13 (2019).
[58] D.L. Postai, C.A. Demarchi, F. Zanatta, D.C.C. Melo, C.A. Rodrigues, Adsorption of rhodamine B and methylene blue dyes using waste of seeds of Aleurites Moluccana, a low cost adsorbent, Alexand. Eng. J. 55 (2016) 1713–1723.
[59] T. Krahnstöver, J. Plattner, T. Wintgens, Quantitative detection of powdered activated carbon in wastewater treatment plant effluent by thermogravimetric analysis (TGA), Water Res. 101 (2016) 510–518.

[60] L.D. Yao, F.Y. Li, J.X. Li, C.Q. Jin, R.C. Yu, Study of the products of melamine (C 3 N 6H 6) treated at high pressure and high temperature, Physica Status Solidi (A) Applic. Mater. Sci. 202 (2005) 2679–2685.
[61] X. Chen, X. Wang, D. Fang, A review on C1s XPS-spectra for some kinds of carbon materials, Fuller. Nanotube. Carbon Nanostruct. (2020) 1048–1058.
[62] R.J.J. Jansen, H. van Bekkum, XPS OF NITROGEN-CONTAINING FUNCTIONAL GROUPS ON ACTIVATED CARBON, 1995.
[63] Y. Kang, Z. Chu, D. Zhang, G. Li, Z. Jiang, H. Cheng, X. Li, Incorporate boron and nitrogen into graphene to make BCN hybrid nanosheets with enhanced microwave absorbing properties, Carbon N Y 61 (2013) 200–208.
[64] L. Százdi, J. Gulyás, B. Pukánszky, Surface characterization of electrochemically oxidized carbon fibers: surface properties and interfacial adhesion, Compos. Interface. 9 (2002) 219–232.
[65] Y. Lu, D. Wu, Y. Qin, Y. Xie, Y. Ling, H. Ye, Y. Zhang, Facile construction of BiOBr/CoAl-LDH heterojunctions with suppressed Z-axis growth for efficient photoreduction of CO2, Sep. Purif. Technol. 302 (2022).
[66] F. Kapteijn, J.A. Moulijn, S. Matzner, H.-.P. Boehm, The development of nitrogen functionality in model chars during gasification in CO and O, 1999.
[67] C. Lin, H. Liu, M. Guo, Y. Zhao, X. Su, P. Zhang, Y. Zhang, Plasmon-induced broad spectrum photocatalytic overall water splitting: through non-noble bimetal nanoparticles hybrid with reduced graphene oxide, Colloid. Surf. A Physicochem. Eng. Asp. 646 (2022).
[68] W. Han, H. Wang, K. Xia, S. Chen, P. Yan, T. Deng, W. Zhu, Superior nitrogen-doped activated carbon materials for water cleaning and energy storing prepared from renewable leather wastes, Environ. Int. 142 (2020).
[69] X. Zhang, H. Li, G. Wang, Q. Ji, T. Liang, Preparation and Characterization of Bio-Nitrogen-Doped Activated Carbon, (2021).
[70] B. Shaku, T.P. Mofokeng, T.H. Mongwe, N.J. Coville, K.I. Ozoemena, M. S. Maubane-Nkadimeng, Physicochemical properties of nitrogen doped carbon nano-onions grown by flame pyrolysis from grapeseed oil for use in supercapacitors, Electroanalysis 32 (2020) 2946–2957.
[71] L. Guan, L. Pan, T. Peng, C. Gao, W. Zhao, Z. Yang, H. Hu, M. Wu, Synthesis of biomass-derived nitrogen-doped porous carbon nanosheests for high-performance supercapacitors, ACS Sustain. Chem. Eng. 7 (2019) 8405–8412.
[72] Y. Lin, H. Zhao, F. Yu, J. Yang, Design of an extended experiment with electrical double layer capacitors: electrochemical energy storage devices in green chemistry, Sustainability (Switzerland) 10 (2018).
[73] R. Heimböckel, F. Hoffmann, M. Fröba, Insights into the influence of the pore size and surface area of activated carbons on the energy storage of electric double layer capacitors with a new potentially universally applicable capacitor model, Phys. Chem. Chem. Phys. 21 (2019) 3122–3133.
[74] V. Pavlenko, S. Kalybekkyzy, D. Knez, Q. Abbas, Z. Mansurov, Z. Bakenov, A. Ng, Revisiting the carbon mesopore contribution towards improved performance of ionic liquid–based EDLCs at sub-zero temperatures, Ionics (Kiel) (2021).
[75] M. Fahim, A. ul H.A. Shah, S. Bilal, Highly stable and efficient performance of binder-free symmetric supercapacitor fabricated with electroactive polymer synthesized via interfacial polymerization, Materials (Basel) 12 (2019).
[76] Y. Lu, S. Zhang, J. Yin, C. Bai, J. Zhang, Y. Li, Y. Yang, Z. Ge, M. Zhang, L. Wei, M. Ma, Y. Ma, Y. Chen, Data on high performance supercapacitors based on mesoporous activated carbon materials with ultrahigh mesopore volume and effective specific surface area, Data Brief 18 (2018) 1448–1456.
[77] F. Barzegar, A. Bello, O. Guellati, D.Y. Momodu, A. Harat, J.K. Dangbegnon, M. Guerioune, N. Manyala, Effect of addition of different carbon materials on hydrogel derived carbon material for high performance electrochemical capacitors, Electrochim. Acta 186 (2015) 277–284.
[78] Z. Sheng, X. Lin, H. Wei, Y. Zhang, Z. Tian, C. Wang, D. Xu, Y. Wang, Green synthesis of nitrogen-doped hierarchical porous carbon nanosheets derived from polyvinyl chloride towards high-performance supercapacitor, J. Power Source. 515 (2021).
[79] X. Wang, M. Lou, X. Yuan, W. Dong, C. Dong, H. Bi, F. Huang, Nitrogen and oxygen dual-doped carbon nanohorn for electrochemical capacitors, Carbon N Y 118 (2017) 511–516.
[80] L. Demarconnay, E. Raymundo-Piñero, F. Béguin, A symmetric carbon/carbon supercapacitor operating at 1.6 v by using a neutral aqueous solution, Electrochem. Commun. 12 (2010) 1275–1278.
[81] S.T. Vindt, E.M. Skou, The buffer effect in neutral electrolyte supercapacitors, Appl. Phys. A Mater. Sci. Process. 122 (2016) 1–6.
[82] A. Virya, K. Lian, A review of neutral pH polymer electrolytes for electrochemical capacitors: transitioning from liquid to solid devices, Mater. Rep.: Energy 1 (2021), 100005.
[83] M.S. Hong, S.H. Lee, S.W. Kim, Use of KCl aqueous electrolyte for 2 V manganese oxide/activated carbon hybrid capacitor, Electrochem. Solid-State Lett. 5 (2002).
[84] Q. Gao, L. Demarconnay, E. Raymundo-Piñero, F. Béguin, Exploring the large voltage range of carbon/carbon supercapacitors in aqueous lithium sulfate electrolyte, Energy Environ. Sci. 5 (2012) 9611–9617.
[85] H. Tomiyasu, H. Shikata, K. Takao, N. Asanuma, S. Taruta, Y.Y. Park, An aqueous electrolyte of the widest potential window and its superior capability for capacitors, Sci. Rep. 7 (2017).
[86] J. Kim, J. Chun, S.G. Kim, H. Ahn, K.C. Roh, Nitrogen and fluorine co-doped activated carbon for supercapacitors, J. Electrochem. Sci. Technol. 8 (2017) 338–343.
[87] H.S. Magar, R.Y.A. Hassan, A. Mulchandani, Electrochemical impedance spectroscopy (Eis): principles, construction, and biosensing applications, Sensors 21 (2021).
[88] G.P. Scisco, M.E. Orazem, K.J. Ziegler, K.S. Jones, On the rate capability of supercapacitors characterized by a constant-phase element, J. Power Source. 516 (2021).
[89] A. Gopalakrishnan, T.D. Raju, S. Badhulika, Green synthesis of nitrogen, sulfur-co-doped worm-like hierarchical porous carbon derived from ginger for outstanding supercapacitor performance, Carbon N Y 168 (2020) 209–219.
[90] C. Chen, M. Zhao, Y. Cai, G. Zhao, Y. Xie, L. Zhang, G. Zhu, L. Pan, Scalable synthesis of strutted nitrogen doped hierarchical porous carbon nanosheets for supercapacitors with both high gravimetric and volumetric performances, Carbon N Y 179 (2021) 458–468.
[91] A.T. Chidembo, K.I. Ozoemena, B.O. Agboola, V. Gupta, G.G. Wildgoose, R. G. Compton, Nickel(ii) tetra-aminophthalocyanine modified MWCNTs as potential nanocomposite materials for the development of supercapacitors, Energy Environ. Sci. 3 (2010) 228–236.
[92] K. Li, J. Luo, M. Wei, X. Yao, Q. Feng, X. Ma, Z. Liu, Functional porous carbon derived from waste eucalyptus bark for toluene adsorption and aqueous symmetric supercapacitors, Diam. Relat. Mater. 127 (2022), 109196.
[93] G. Ma, D. Guo, K. Sun, H. Peng, Q. Yang, X. Zhou, X. Zhao, Z. Lei, Cotton-based porous activated carbon with a large specific surface area as an electrode material for high-performance supercapacitors, RSC Adv. 5 (2015) 64704–64710.
[94] H. Gou, J. He, G. Zhao, L. Zhang, C. Yang, H. Rao, Porous nitrogen-doped carbon networks derived from orange peel for high-performance supercapacitors, Ionics (Kiel) 25 (2019) 4371–4380.
[95] P. Song, X.P. Shen, X.M. He, K.H. Feng, L.R. Kong, Z.Y. Ji, L.Z. Zhai, G.X. Zhu, D. Y. Zhang, Cellulose-derived nitrogen-doped hierarchically porous carbon for high-performance supercapacitors, Cellulose 26 (2019) 1195–1208.